

ELECTRON TEMPERATURES OF THE CORONA ABOVE A SOLAR ACTIVE REGION DETERMINED FROM S XV SPECTRA

ALPHONSE C. STERLING¹

Computational Physics Inc., 2750 Prosperity Avenue, Suite 600, Fairfax, VA 22031; asterling@solar.stanford.edu

HUGH S. HUDSON¹

Solar Physics Research Corp., 4720 Calle Desecada, Tucson, Arizona 85718; hudson@solar.stanford.edu

AND

TETSUYA WATANABE

National Astronomical Observatory, Mitaka, Tokyo 181, Japan; watanabe@spot.mtk.nao.ac.jp

Received 1996 December 10; accepted 1997 January 31

ABSTRACT

We present the first high-resolution soft X-ray spectral observations of the corona above an active region, using the Bragg crystal spectrometer (BCS) on board the *Yohkoh* satellite. We observed NOAA AR 7978 as it rotated beyond the solar limb so that the lower portions of the region were occulted. Long integrations from times after the region had totally disappeared some days later show a substantial, variable background in S xv. Since the background spectrum is featureless, spectral lines obtained from the time of occultation must originate from the upper corona of the active region. Our results support previous findings that the active region corona consists of two components: a cooler, steady component with $T_e \approx 3$ MK and a hotter, transient component in excess of 5 MK. This hotter component is due to microflares; outside the time of microflares there is relatively little or no active region upper coronal plasma with $T_e \gtrsim 3.5$ MK. There is evidence for a decrease in T_e with height for the cool component.

Subject headings: Sun: corona — Sun: flares — Sun: X-rays, gamma rays

1. INTRODUCTION

High-resolution X-ray spectroscopy can provide a powerful method for deriving electron temperatures and other spectral properties of the corona of active regions. Watanabe et al. (1992, 1995) have carried out such studies for periods when there were several active regions on the Sun, using the helium-like sulfur (S xv) channel of the Bragg Crystal Spectrometer (BCS) on board *Yohkoh*. Since BCS has no spatial resolution, however, it was not possible to isolate the properties of an individual active region in the Watanabe et al. studies. Rather, all the active regions, along with the bright background soft X-ray corona, contributed to the spectra that they analyzed. Sterling (1997) was able to deduce spectral properties of an individual active region by using data from a quieter period when a single active region was present and the background coronal flux was low. In this *Letter*, we describe the use of the solar limb as an occulting edge to restrict the BCS observations of an active region even further, namely, to the upper regions of the corona above the active region. We believe our result is the first determination of the electron temperature in the high-altitude corona of an active region using narrowband soft X-ray spectra. Our findings have implications on the role of X-ray microflares in coronal heating. They are also of interest in light of ongoing coronal studies with the *Yohkoh* and *SoHO* satellites.

Recently, the procedure of using the solar limb as an occulting edge has been used effectively to study spectral properties of the upper regions of flaring loops (Khan et al. 1995; Mariska, Sakao, & Bentley 1995; and Sterling et al. 1996, 1997). In those flare studies, the background emission was

always much greater than that from the detector background. We find here, however, that the intensity level of a partially occulted active region can be comparable to that of the detector background in the BCS S xv channel. This background and its variability will have to be considered when analyzing data from weak sources, which are likely to occur during the current solar minimum period.

2. INSTRUMENTS AND DATA

For this study we limit our spectral data to that from the S xv channel of BCS (approximately covering the wavelength range 5.0160–5.1143 Å). Although BCS has three higher energy channels—Fe xxvi (1.7636–1.8044 Å), Fe xxv (1.8298–1.8942 Å), and Ca xix (3.1631–3.1912 Å)—only the S xv channel routinely observes flux from nonflaring active region plasmas. BCS utilizes two one-dimensional position-sensitive proportional counter detectors. Culhane et al. (1991) and Lang et al. (1992) give detailed descriptions of the *Yohkoh* BCS. We also use imaging data from *Yohkoh*'s Soft X-ray Telescope (SXT; Tsuneta et al. 1991).

The active region of this study was designated AR 7978 by the National Oceanic and Atmospheric Administration (NOAA). It arose at the site of a long-lived complex of activity and became prominent on the solar disk on 1996 July 6. Except for a short period, it was the only active complex for several months.

3. ANALYSIS

Inspection of data from *GOES* photometers shows a drop in the X-ray flux when AR 7978 rotated behind the west limb, dropping from about 10^{-4} erg cm⁻² s⁻¹ in the *GOES* 1–8 Å channel (*GOES* B level) prior to \approx July 14 to well below 10^{-5}

¹ Current address: Institute for Space and Astronautical Science, Yoshinodai 3-1-1, Sagami-hara, Kanagawa 229, Japan.

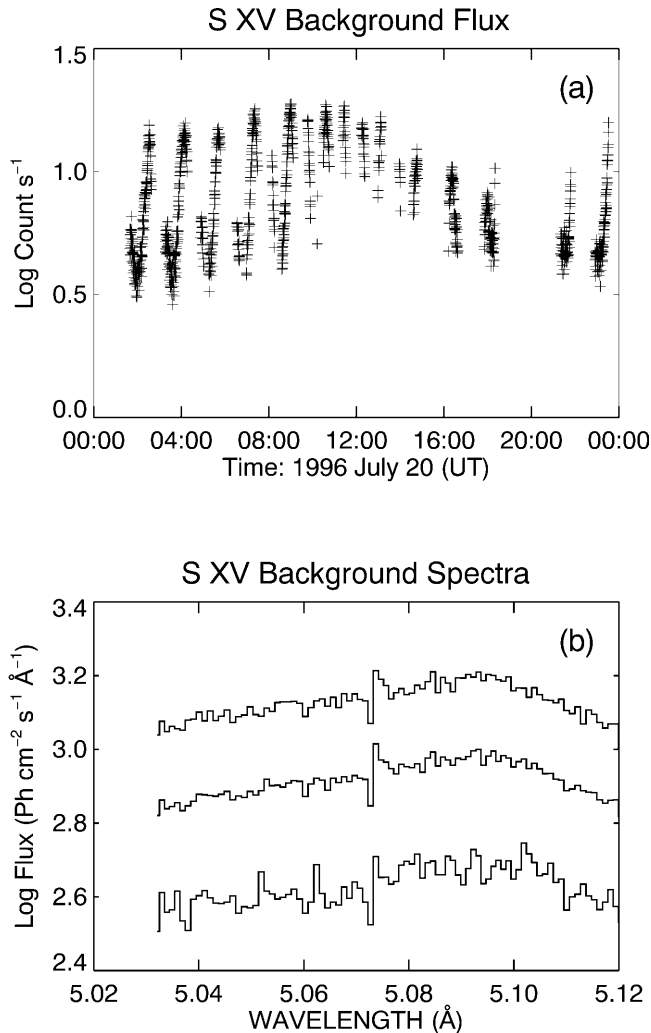


FIG. 1.—(a) S xv flux as a function of time during a period when there were no active regions on the solar disk on 1996 July 20. The cyclical variation seems to be related to *Yohkoh*'s orbital period. (b) Spectra accumulated from the 1996 July 20 data for intensity levels with $\log \text{count s}^{-1} \leq 0.7$ (bottom), ≥ 1.0 (top), and for the average from the entire period (middle). The feature at 5.73 \AA is a detector artifact. Wavelength scale is offset (to account for north-south source position; see, e.g., Sterling 1997) the same amount as for the spectra in Fig. 4.

$\text{erg cm}^{-2} \text{ s}^{-1}$ (*GOES* A level) after \approx July 15. Not until July 25, when the region began to reappear around the east limb, did the flux again climb and remain above the *GOES* A level. Before embarking on an examination of the spectra from the partially occulted active region, we first investigate the nature of background emissions detected in S xv when the active region is not on the disk.

Figure 1a shows the S xv intensity on July 20, where each datum is from a spectrum accumulated for 24 s. Even during this very quiet period there is always a background spectrum present, and this contribution will have to be removed when flux from the features we are trying to observe are weak. This background seems to vary cyclically as a function of time with a period related to the 96 minute orbit of *Yohkoh*, suggesting a terrestrial origin. We have found similar flux levels and cyclical variations throughout the period 1996 July 16–24, when the active region is not on the solar disk. Figure 1b shows three spectra obtained from July 20, where the bottom spectrum is derived by accumulating data with $\log \text{count s}^{-1} \leq 0.7$

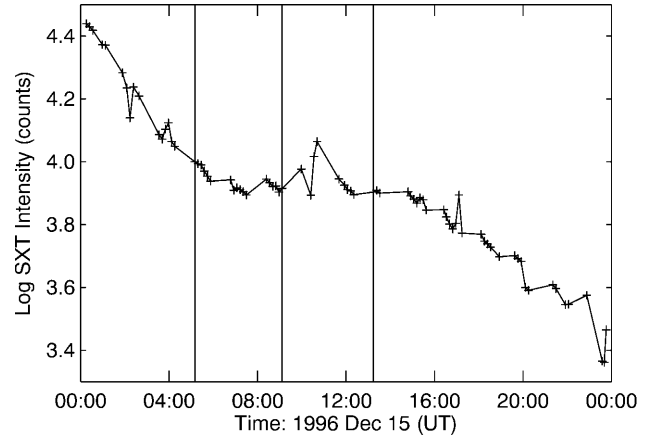


FIG. 3.—Integrated intensity from SXT images of AR 7978 as a function of time. As the region disappears around the limb, the flux reduces virtually monotonically, except for a microflare (*GOES* level A2) near 11 UT. From the left, the four regions defined by the vertical lines mark off the integration periods used for spectra in Figs. 4a–4d, respectively.

(Fig. 1a), the top spectrum is from data with $\log \text{count s}^{-1} \geq 1.0$, and the middle spectrum is an average over the entire period. These three spectra were accumulated for 6888, 7920, and 24,720 s, respectively. Thus, the background spectrum can vary in intensity by a factor of 3 or 4 over time, but its shape (on a log scale) is nearly unchanged.

In analyzing S xv spectra, the prominent lines of concern are the resonance line at 5.04 \AA (line *w* in the notation of Gabriel 1972), the “d13 complex” near 5.05 \AA , and the line complex near 5.10 \AA consisting of two dielectronic lines (lines *j* and *k*) and a forbidden line (line *z*). We see no evidence for resolved spectral lines in the background spectra at these (or at any other) wavelengths for the three Figure 1b spectra. Rather, each spectrum has a slight maximum near 5.10 \AA . We do not know the origin of this background, but its shape is similar to the background due to fluorescence seen in the BCS Fe xxvi channel spectra, even during the time of flares (see Pike et al. 1996).

Figure 1b shows that the background spectrum maintains its shape and can be derived by a multiplicative factor times the mean spectrum to within a few percent across the whole spectral range. (Variations in the daily mean spectra between 1996 July 16–24 are within about 20% over the spectral range, i.e., there seems to be little variation in the average background over the time periods considered here.) We therefore simply vary the average background spectrum's intensity when removing it from our partially occulted active region spectra. Since the background spectra show no clear spectral lines, and because their accumulation times are comparable to those that we will take during the occultation time in the forthcoming analysis, any spectral lines seen during the occultation time must originate from the active-region corona.

Figure 2 (Plate L11) shows SXT AIMg filter images for the region as it disappears behind the west limb at four different times on July 15. Each image is $628 \times 628 \text{ arcsec}^2$ with $9''.82$ pixels, and the exposure times are 5.338 s in Figures 2a, 2c, and 2d and 0.668 s in Figure 2b. Intensities in each panel of Figure 2 are normalized separately, so intensity differences between panels are not real. Figure 3 shows the actual variation of the SXT flux integrated over the region shown in the images of Figure 2, as a function of time for times when the flux drops as the region rotates over the limb. This flux is generally smoothly

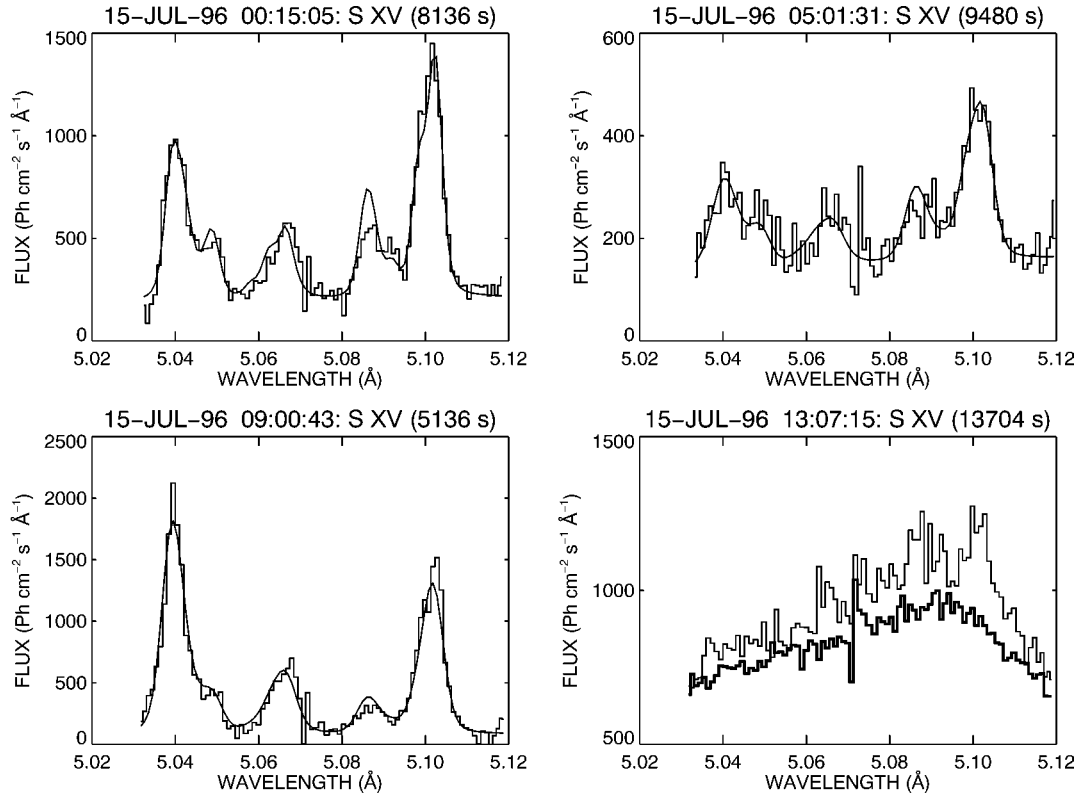


FIG. 4.—Spectra (*histograms in [a]–[c], thin-line histogram in [d]*) accumulated over four time periods: (a) 00:09–05:01 UT, (b) 05:01–09:00 UT, (c) 09:00–13:07 UT, and (d) 13:07–23:39 UT. A background spectrum has been removed in (a)–(c). In (d) the thick-line histogram is an average background spectrum. Resulting best-fit spectra (*solid line*) have T_e -values of 3.4 ± 0.02 , 3.1 ± 1.1 , and 6.2 ± 1.8 in (a)–(c), respectively, and in (d) emissions in excess of background indicate $T_e \approx 2.0$ – 2.5 MK.

decreasing, except for a sharp jump near 11 UT. This is a microflare-type feature, which has a *GOES* flux value of about A2. Figures 2a and 2b are from times prior to the microflare, showing brightenings near the limb and more nebulous material at greater heights. Figure 3c is from a time when the microflare is brightening and shows that this microflare also occurs at a location near the limb. Finally, Figure 2d is from a time after occurrence of the microflare where the flux is much reduced and almost monotonically declining. In contrast to the three earlier panels, there are no outstanding brightenings near the solar limb at the time of the Figure 2d image. Features seen in that panel must be at high altitudes above the active region. Figure 3 suggests that no major brightenings occur after about 12:30 UT, since the flux shows no substantial jumps (except for a small brightening near 16 UT). Movies made from SXT images indicate that there are many dynamic changes during the last time period, perhaps indicating formation of new loops, weak transient brightenings (e.g., Shimizu 1995) or intensity changes in pre-existing loops. All these intensities, however, are very weak compared to those of earlier times (see Fig. 3).

Figure 4 shows S XV spectra (*histograms*) corresponding to the four images in Figure 2. Spectra in Figures 4a, 4b, 4c, and 4d are made by accumulating spectra for 8136, 9480, 5136, and 13704 s, respectively, corresponding to data available during the four time intervals 00:15–05:01 UT, 05:01–09:00 UT, 09:00–13:07 UT, and 13:07–23:39 UT, respectively (delineated by the vertical lines in Fig. 3). For the spectra in Figures 4a–4c we have subtracted, respectively, 0.5, 0.5, and 1.0 times the average background spectrum in Figure 1b, so that the

continuum levels near 5.055 and 5.080 Å are nearly identical as expected from theoretical spectra. Despite the long accumulation time, the spectrum from the final time period is extremely weak. In Figure 4d, we therefore plot the non-background-subtracted spectrum (*thin-line histogram*) and overplot the average background from Figure 1b (*thick-line histogram*).

Overplotted as solid lines over the background-removed, observed spectra in Figures 4a–4c are best-fitting theoretical spectra resulting from a minimized χ^2 analysis. Atomic data for the synthetic spectra are from Harra-Murnion et al. (1996), fractional ionization values are from Arnaud & Rothenflug (1985), and we take a sulfur abundance of 8.6×10^{-6} . Similar to Sterling (1997), we limit our fits to wavelength ranges between approximately 5.025 and 5.055 Å, and between 5.094 and 5.110 Å; the intensity ratio between these two regions is a sensitive indicator of electron temperature, T_e . From these fits we deduce T_e -values of 3.4 ± 0.02 , 3.1 ± 1.1 , and 6.2 ± 1.8 MK for spectra in Figures 4a, 4b, and 4c, respectively, where the uncertainties are the 1σ levels resulting from the fits. Each of these fits have reduced χ^2 -values under 1. In addition, there are uncertainties due to our background selection. We estimate the magnitude of this effect by making spectral fits using 20% more and 20% less of the background removed in our basic calculation for the spectra of Figures 4a–4c. This results in variations in T_e of ± 0.1 MK for spectra in Figures 4a and 4b, and T_e -values between 5.4 and 7.6 MK for the Figure 4c spectrum. (The relatively large range in values for the Fig. 4c spectrum is probably due to the time variability of the microflare over the integration time; see Fig. 3.)

Because of the weakness of the spectrum of Figure 4*d*, it is difficult to obtain precise temperatures. We can fit the emissions in excess of background near 5.10 and 5.04 Å with synthetic spectra between 2.0 and 2.5 MK.

Spectral line broadenings in excess of those expected from thermal effects are often discussed in terms of a nonthermal velocity (v_{nt}). As described elsewhere (e.g., Sterling 1997), estimates for v_{nt} from BCS are affected by the spatial extent of the emitting soft X-ray source in the north-south direction. Using composite SXT AlMg images superimposed over four time ranges close to those of the spectra in Figure 4, we estimate that this north-south spatial contribution is comparable to the derived v_{nt} -values in all cases except Figure 2*c* (which has $v_{nt} = 160 \pm 50 \text{ km s}^{-1}$). Therefore, we are unable to determine reliable v_{nt} -values for the nonmicroflaring corona. SXT Be images are more appropriate than AlMg images in making this comparison, but none are available for this data set.

4. RESULTS AND DISCUSSION

We find T_e -values in the over-the-limb active region to be near 3 MK at all times, except when the microflare occurs. At that time T_e jumps to values in excess of 5 MK. Even qualitatively, the strong dominance of the intensity of the line feature near 5.10 Å over that of the resonance line in Figures 4*a*, 4*b*, and 4*d* indicates a temperature no higher than 3–4 MK, while the dominance of the resonance line over the 5.10 Å line feature in Figure 4*c* indicates that T_e is near or in excess of 5 MK (Harra-Murnion et al. 1996). Since the contribution function for S xv peaks near 15 MK (Doschek 1990), our findings indicate that there is little or no plasma with $T_e \gtrsim 3.5$ MK in the corona above active regions outside the times of microflares. (Using SXT data, Klimchuk & Gary 1995 find higher T_e -values in apparently nonmicroflaring coronal loops; our results imply that emission measure of cooler plasma dominates any such hotter plasma.) Since the resonance line is nearly absent in Figure 4*d* our results suggest a decrease in average temperature of the corona with height (in agreement with Mosher 1979, and Klimchuk & Gary 1995) above this active region.

We have found that the quiet Sun without active regions does not register a significant line spectrum in S xv, even when accumulated for nearly 7 hr. This nonsolar background must be taken into consideration in analyzing extremely low flux BCS spectra, or when studying abundances (in which case the

continuum is very important; see, e.g., Sterling 1996). We do not know how this background appears outside the period of time discussed in this Letter. (Sterling 1997 did not remove this background, but his results are probably not affected too much by background since spectra with poor χ^2 -values were rejected.) Also, it may be that the Sun without active regions during a more active phase of the solar cycle has a more intense S xv signature.

Using temperature diagnostics from SXT, Yoshida & Tsuneta (1996) suggest a two-temperature component structure to the active region corona, with a transient hot component and a more steady cool component (Porter & Klimchuk 1995 make a similar suggestion). Our results from BCS strongly support these findings, with the cool component having a temperature of about 3 MK. We also find the loops that appear bright in Figures 2*a* and 2*b* to be within 1 or 2 MK of the dimmer loops seen in Figure 2*d*, confirming a similar finding of Yoshida & Tsuneta. Higher temperatures occur only during the time of the microflare near 11 UT in this data set.

Brightenings and the microflare in Figures 2*a*–2*c* occur near the limb and therefore probably at low heights in the active region. Presumably, they originate from low-lying (i.e., short length) coronal loops; the relatively sharp fall-off of intensity as the occultation progresses (Fig. 3) suggests a well-defined upper limit to their length. In contrast, only higher (i.e., longer) loops are visible in Figure 2*d*, and they may be showing loop-top brightenings, similar to those discussed in connection with flares (e.g., Feldman et al. 1994; Doschek, Strong, & Tsuneta 1995). Our finding that, outside the time of microflares, T_e in the short loops (which presumably dominate the S xv emission for the times of Figs. 2*a* and 2*b*) is about the same as or slightly hotter than in the long loops (Fig. 2*d*) suggests that the reduced flux of the long loops (Fig. 3) must result principally from a reduced density in the long loops compared to the short loops. This follows from the scaling law of Rosner, Tucker, & Vaiana (1978), $T_{\max} \sim (pL)^{1/3}$, (where T_{\max} , p , and L are the maximum T_e , pressure, and loop length, respectively), since intensity in SXT images is a response to p . (It also follows using the somewhat different scaling relationship observed by Kano & Tsuneta 1995.)

The authors thank L. Harra-Murnion and K. Phillips for useful discussions. A. C. S. acknowledges support from the NRL/ONR basic research program. H.S.H. received support from NASA under contract NAS 8-37334.

REFERENCES

- Arnaud, M., & Rothenflug, R. 1985, *A&AS*, 60, 425
 Culhane, J. L., et al. 1991, *Sol. Phys.*, 136, 89
 Doschek, G. A. 1990, *ApJS*, 73, 117
 Doschek, G. A., Strong, K. T., & Tsuneta, S. 1995, *ApJ*, 440, 370
 Feldman, U., Seely, J. F., Doschek, G. A., Strong, K. T., Acton, L. W., Uchida, Y., & Tsuneta, S. 1994, *ApJ*, 424, 444
 Gabriel, A. H. 1972, *MNRAS*, 160, 99
 Harra-Murnion, L., et al. 1996, *A&A*, 308, 670
 Kano, R., & Tsuneta, S. 1995, *ApJ*, 454, 934
 Khan, J. I., Harra-Murnion, L., Hudson, H. S., Lemen, J. R., & Sterling, A. C. 1995, *ApJ*, 452, L153
 Klimchuk, J., & Gary, D. E. 1995, *ApJ*, 448, 925
 Lang, J., et al. 1992, *PASJ*, 44, L55
 Mariska, J. T., Sakao, T., & Bentley, R. D. 1995, *ApJ*, 459, 815
 Mosher, J. M. 1979, *Sol. Phys.*, 64, 109
 Pike, C. D., et al. 1996, *ApJ*, 464, 487
 Porter, L. J., & Klimchuk, J. A. 1995, *ApJ*, 454, 499
 Rosner, R., Tucker, W., & Vaiana, G. 1978, *ApJ*, 220, 643
 Shimizu, T. 1995, *PASJ*, 47, 251
 Sterling, A. C. 1996, in *Workshop on High Energy Solar Physics*, ed. R. Ramaty, N. Mandzhavidze, & X. M. Hua (New York: AIP), 343
 ———. 1997, *ApJ*, in press
 Sterling, A. C., Harra-Murnion, L. K., Hudson, H. S., & Lemen, J. R. 1996, *ApJ*, 464, 498
 Sterling, A. C., Hudson, H. S., & Lemen, J. R., & Zarro, D. A. 1997, *ApJS*, in press
 Tsuneta, S., et al. 1991, *Sol. Phys.*, 136, 37
 Watanabe, T., et al. 1992, *PASJ*, 44, L141
 ———. 1995, *Sol. Phys.*, 157, 185
 Yoshida, T., & Tsuneta, S. 1996, *ApJ*, 459, 342

FIG. 2.—Images from *Yohkoh's* SXT showing AR 7978 as it rotates around the west limb. Each image was taken with the AlMg filter, and each panel size is 628×628 arcsec². Some of the brightest pixels are saturated. A microflare occurs near the time of (c). Intensity is independently scaled in each frame; the absolute intensity of (d) is much lower than the three earlier images (see Fig. 3).

STERLING, HUDSON, & WATANABE (see 479, L150)